Asian Journal of Chemistry; Vol. 36, No. 11 (2024), 2593-2597

ASIAN JOURNAL OF CHEMISTRY

https://doi.org/10.14233/ajchem.2024.32512

Preparation, Characterization and Conductivity of SiO_2 doped rGO-WO_3 Composite for Battery Application

R. RAVICHANDRAN[1], S. DARLIN QUINE[1,*], S. SHARMILA QUEENTHY[2] and ILAVARASAN M. DHAMU[3]

[1]Department of Chemistry, Government Arts College (Affiliated to Thiruvalluvar University, Vellore), C. Mutlur, Chidambaram-608102, India
[2]Department of Chemistry, Saveetha Engineering College, Saveetha Nagar, Thandalam, Chennai-602105, India
[3]Saveetha Medical College and Hospital, Thandalam, Chennai-602105, India

*Corresponding author: E-mail: chemdar123@gmail.com

Received: 16 August 2024; *Accepted*: 15 October 2024; *Published online*: 30 October 2024; AJC-21794

High-performance solid polymer electrolytes are regarded as one of the most promising materials to be used in the development of lithium ion batteries with improved extended life, increased recyclability and increased safety for electric vehicles and energy storage. In this work, a microwave-assisted hydrothermal technique was used to produce SiO_2-doped rGO-WO_3 composite, which possesses outstanding supercapacitor capabilities. This method is simple, low-cost method without using any other capping and reducing agents. The obtained SiO_2 doped rGO-WO_3 composite structural, morphology and components have been examined by XRD, FT-IR, FE-SEM, TEM, EDX, UV-visible techniques. It was found that the SiO_2 doped rGO-WO_3 composite well crystalline and the size range is about 20-30 nm. The SEM morphology results showed that the nanoparticles were stabilized by rGO, having cavity like structure and randomly distributed on the rGO-WO_3 matrix. The solid state electrolyte revealed superior lithium ion transference number and cyclic stability. The SiO_2 doped rGO-WO_3 composite shows improved ionic conductivity of 2.74×10^{-5} S cm^{-1} at room temperature.

Keywords: Solid polymer electrolyte, Battery, Conductivity, Morphology study.

INTRODUCTION

Developing materials with charge storage capacity, rapid response time, high durability, high power density and long life cycle is a major focus of engineering and scientific research due to the increasing use of renewable energy sources [1-3]. The electrochemical materials with high power and low-cost energy storage devices and their application can be found in solar, wind, hybrid cars, power supply and renewable energy system. Modern Li-ion batteries have been used in a lot of portable electronics and electric cars during the last few decades. This is because of its good life cycle, high energy density and environmental friendliness [4-7]. However, most of the commercially available Li-ion batteries are high energy density but higher safety risk and lower thermal stability [8,9]. Critical safety issues are one of the biggest problems in Li-ion batteries based on liquid organic electrolyte, which has a low flash point around room temperature [10]. Although, solid-state electrolyte has shown a safer alternative to liquid electrolyte due to leakage free, non-flammability, non-volatility and production of high energy density [11-13].

Among various metal oxides, WO_3 belongs to the II-VI semiconductor material which are have wide band gap of 3.0 eV and large excitation binding energy of 284 eV [14,15]. The key advantages of WO_3 are low cost, visible light catalyst, good sensor, easy availability and high stability [16,17]. WO_3 is also commonly used in UV lasers, solar cells, emitting diodes, dyes, adhesives, sensors. However, the poor rate capability and capacity retention is an important challenge for the solid-supercapacitor application. To overcome this problem, we prepared the composite is hybridization of rGO with WO_3. The rGO is a atomic-scale, honey-comb, two-dimensional structure. This is an exceptional optical, thermal, electronic application due to grate chemical and mechanical stability, high specific area [18,19].

Thus, we propose to synthesize the SiO_2 doped rGO-WO_3 (1:1 ratio) by microwave-assisted hydrothermal method with high crystalline, enhanced supercapacitor application. The

produced nanoparticles and composites underwent extensive structural and SEM morphological investigations. The elemental composition and SEM morphology of the solid state electrolyte were examined using EDAX and field emission scanning electron microscopy (FESEM), respectively. Through the use of electronic impedance spectroscopy (EIS), the conductivity studies were computed.

EXPERIMENTAL

Reduced graphene oxide (rGO), sodium tungstate ($Na_2WO_4 \cdot 2H_2O$), sodium bisulfate ($NaHSO_4 \cdot H_2O$) and tetraethyl silicate ($(C_2H_5)_4SiO_2$ were purchased from Sigma Aldrich in AR grade. Ethanol was purchased from Chem-O-Chem chemicals. All reagents were used without further purification.

WO_3 nanoparticles preparation: The hydrothermal synthesis was used to synthesize WO_3 nanoparticles, In brief, 2 g of $NaHSO_4$, 1 g of $Na_2WO_4 \cdot 2H_2O$ and 50 mL of distilled water were mixed vigorously for 30 min. After transferring the yellow-coloured mixture into a Teflon autoclave, heated it to 150 ºC for 24 h and then the precipitation was allowed to mature for another 24 h at ambient temperature. Ultimately, the precipitate was recovered by centrifugation and the sample was then baked for 3 h at 500 ºC.

Preparation of SiO_2 doped rGO-WO_3 composites: The synthesis of SiO_2-doped rGO-WO_3 composite was carried out using a microwave-assisted hydrothermal technique. To obtain a homogenous solution, 2.31 g of WO_3 and 2 g of tetraethyl silicate were dispersed in 100 mL of a mixed solution that contained 85 mL of deionized water and 15 mL of sodium bisulfate. The mixture was then sonicated for 1 h. After dissolving 2.04 g of rGO in deionized water, the mixture was magnetically swirled for 1 h. Every precursor was placed in a microwave oven and heated for 15 min, after stirring for 1 h. In order to improve the crystallinity, the resulting SiO_2 doped rGO-WO_3 was finally washed with ethanol followed by deionized water until become neutralized and finally dried for 2 h at 500 ºC in an oven.

Characterization: Using an X-ray diffraction (XRD) pattern obtained on a Bruker D8 Advance (Germany) with Cu*K*α radiation (λ = 1.5406 Å) at an acceleration voltage of 40 kV and a diffraction angle 2θ range of 10º to 80º, the crystalline nature of the produced nanoparticles and nanocomposite was studied. Fourier transform infrared (FT-IR) spectra were obtained using the KBr pellets methods (Perkin-Elmer 1725 spectrometer, USA) in the 400-4000 cm^{-1} wavenumber range in order to study the existence of nanoparticles and nanocomposite. The field emission scanning microscope (FESEM) images of the nanoparticles and nanocomposite were obtained using an FEI-Quanta FEG 200F (Netherlands) microscope running at an accelerating voltage of 30 kV and equipped with energy dispersive X-ray (EDX) spectra for elemental analysis. Using a reflectance sample of $BaSO_4$, the optical characterization was performed in the 200-500 nm range using a Cary 100 UV-visible spectrophotometer (USA) to estimate the energy band of the sample.

Electrochemical impedance spectroscopy: Electronic impedance spectroscopy was used using a CHI 660 electrochemical workstation to calculate the conductivity and activation energy. The ionic conductivity (σ) was measured with amplitude of 5 mV for open circuit potential and in the frequency range of 10 Hz – 100 kHz and temperature range of 25 ºC to 70 ºC. The membranes were placed between the stainless steel (SS) electrodes at room-temperature. Using the high frequency AC impedance approach, the conductivity (σ) was determined using the following formula [20,21]:

$$\sigma = \frac{L}{(R,S)}$$

where L, R and S correspond to the thickness of the polymer electrolyte, bulk resistance and area of the stainless steel (SS) electrode, respectively.

Discharge characteristics: In battery, the cathode consists of graphite (C) whereas the anode is composed of solid polymer lithium electrolyte. The cell's discharge characteristics were examined under a 100 KΩ load. A number of battery-related cell metrics were evaluated including the power density, energy density, current density, short circuit current (SCC) and open circuit voltage (OCV).

RESULTS AND DISCUSSION

Structural and morphology properties: The crystallinity and crystal phases of prepared pure WO_3 and SiO_2 doped rGO-WO_3 were analyzed by XRD studies (Fig. 1). The appearance of six strong characteristic diffraction peaks at 2θ = 13.52º, 22.26º, 25.48º, 35.14º, 50.42º, 55.34º were assigned to the (101), (001), (200), (201), (220), (202) planes of WO_3 crystalline with hexagonal structure (JCPDS No: 85-2460) (Fig. 1a). In SiO_2-doped rGO-WO_3 (Fig. 1b), a distinct diffraction peak is found at 26.45º and 54.61º, corresponding to the (002) plane, which is associated with rGO, moreover, the common diffraction peaks of WO_3 were also appeared. The peak intensity of WO_3 is marginally lower in the SiO_2-doped rGO-WO_3 comp-

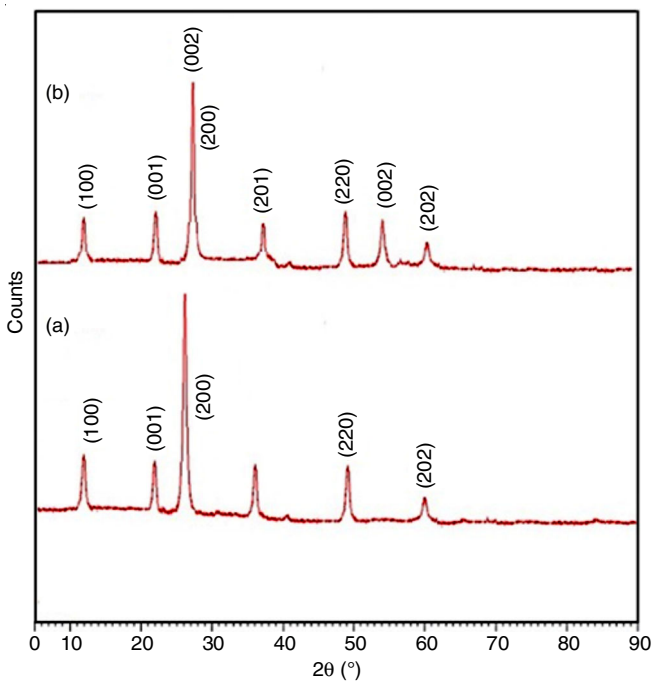

Fig. 1. Powder XRD pattern of (a) WO_3 (b) SiO_2 doped rGO-WO_3 composite

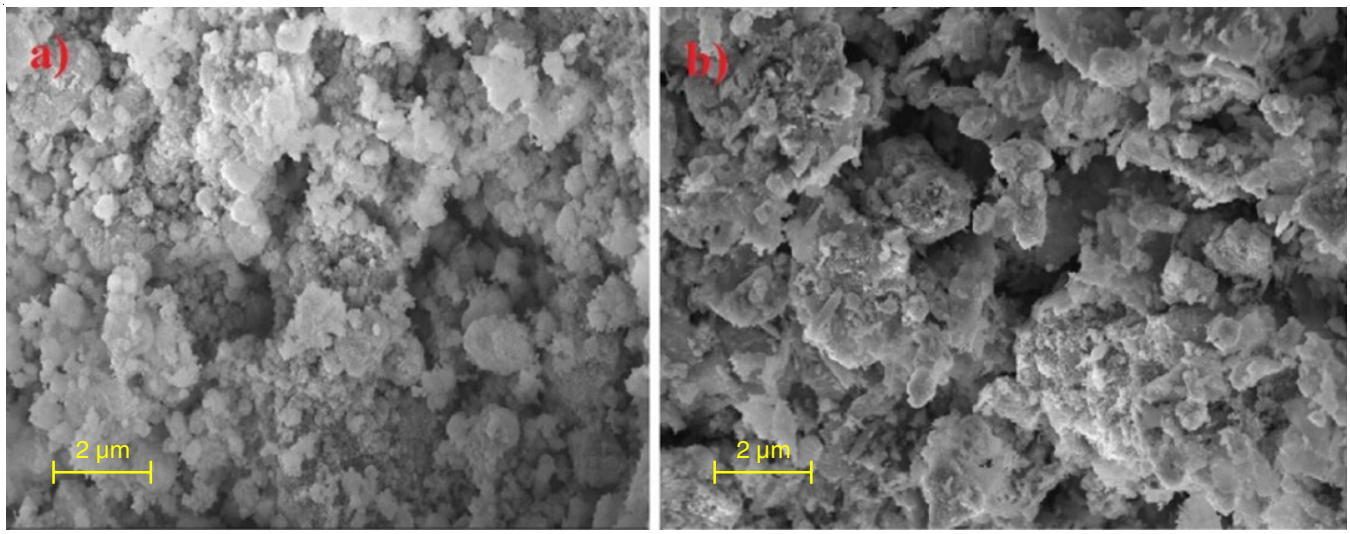

Fig. 2. Powder FE-SEM images of (a) WO_3 (b) SiO_2 doped rGO-WO_3 composite

osite suggesting that the diffusion of SiO_2 and rGO into the WO_3 crystalline region has partially destroyed its crystallinity. The particle sizes of pure WO_3 and SiO_2-doped rGO-WO_3 composite were determined using the Debye-Scherrer formula, yielding the mean crystalline sizes of around 32 nm and 24 nm, respectively.

The surface morphology and physical properties of pure WO_3 and SiO_2-doped rGO-WO_3 composite were examined *via* FE-SEM analysis. Fig. 2a illustrates that the images of pure WO_3 exhibit a slight qualitative difference in porous and spherical structures. The HR-SEM images of SiO_2 doped rGO-WO_3 (Fig. 2b) revealed that the samples exhibit a spherical morphology, alongside a sheet-like structure associated with rGO, with no observable aggregation among the particles. Significantly, the nanocomposite architecture is facilitated by the rGO matrix fiber framework, wherein WO_3 nanoparticles exhibit interfacial interactions with the rGO matrix. The detection of carbon, oxygen, hydrogen, silica and tungsten elements in SiO_2 doped rGO-WO_3 indicates that the prepared composite was successfully formed.

FT-IR spectral studies: The chemical structure of pure WO_3 and SiO_2 doped rGO-WO_3 composite were analyzed by FT-IR spectra. Fig. 3 shows the characteristic peaks of WO_3 appear in 1476- 559 cm^{-1} region attributed to the vibration mode of W-O and C=O stretching vibration mode [22,23]. In SiO_2 doped rGO-WO_3 composite, the FT-IR peaks at 559 cm^{-1}, 856 cm^{-1}, 1476 cm^{-1}, 1645 cm^{-1} and 3443 cm^{-1} were correspond to W-O, C=O stretching vibration, C=C skeletal vibration, C-O stretching vibration, O-H water vibration, respectively. As can be seen in FT-IR result of composite C=C and O-H stretching vibration appeared, which is confirm the formation of rGO-WO_3 composite.

UV-Visible spectral studies: Fig. 4 shows the UV-visible spectra of pure WO_3 and SiO_2 doped rGO-WO_3 composite samples. A broad reflection band at 456 nm was attributed to the absorption peak of WO_3 nanoparticles and at 485 nm for SiO_2 doped rGO-WO_3 composite confirmed the impregnation of rGO matrix in the formation of SiO_2 doped rGO-WO_3 com-

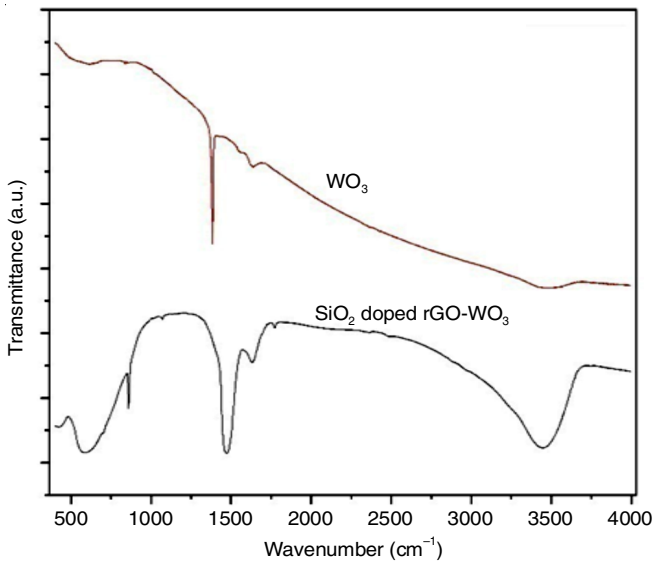

Fig. 3. FT-IR spectra of WO_3 and SiO_2 doped rGO-WO_3 composite

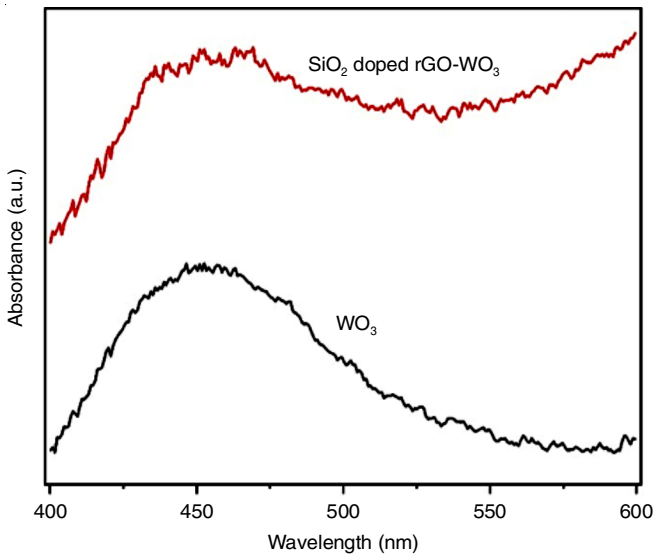

Fig. 4. UV-Visible spectra of WO_3 and SiO_2 doped rGO-WO_3 composite

posite. Based on the absorption spectra, the optical band gap of the samples was determined from the Kubelka-Munk function $\alpha h\nu = A(h\nu - E_g)^{1/2}$ with ν is the frequency of light, h is Plank's constant, A is the absorbance, E_g is the optical band gap [22,23]. The band gap energies of WO_3 and SiO_2 doped rGO-WO_3composite were found to be 2.96 and 2.74 eV, respectively.

Ionic conductivity

Electronic impedance spectroscopy: The ionic conductivities of the samples were analyzed using electrochemical impedance spectroscopy (EIS) using a three electrode setup at room temperature. At room temperature or at 30 ºC, the electrolyte conductivity (σ) of solid state composite was computed. Table-1 displays the addition of SiO_2 and rGO to the WO_3 nanoparticles along with the related conductivity values. The composition of SiO_2-doped rGO-WO_3 composite demonstrates a high conductivity value of 2.74×10^{-5} S cm^{-1}. The incorporation of SiO_2 and rGO into WO_3 nanoparticles improved the conductivity. The addition of rGO to WO_3 also increases the amorphous phase and generates segmental mobility in the hexagonal phase, both of which improve the ionic conductivity. Incorporating SiO_2 as a filler into the rGO matrix enhances the conductivity due to the dissociation of metal ion aggregates into free ions, even though this is caused by the composite effect and the formation of a conducting space-change double layer between the WO_3 nanoparticles and solid state electrolytes.

TABLE-1
IONIC CONDUCTIVITY VALUES OF POLYMER ELECTROLYTES WO_3 AND SiO_2 DOPED rGO-WO_3 AT ROOM TEMPERATURE

Sample	Conductivity at room temperature (S/cm)
Pure WO_3	5.84×10^{-9}
SiO_2 doped rGO-WO_3	2.74×10^{-5}

Additionally, the ionic conductivity (σ) values of the WO_3 and SiO_2-doped rGO-WO_3 composite electrolytes were determined and displayed in Fig. 5. The ionic conductivity of the synthesized composite seems to be increasing; however, the ionic conductivity of the solid-state electrolytes is improved by the combination of rGO and SiO_2. Solid state composite electrolytes have excellent ionic conductivity values at ambient temperature, which makes the sample a potential material for the development of solid-state electrochemical devices such lithium ion batteries.

Discharge characteristics: The SiO_2-doped rGO-WO_3 composite solid state electrolytes were used to fabricate a solid state electrolyte battery and their discharge characteristics were assessed (Fig. 6). The lithium (anode), SiO_2-doped rGO-WO_3 composite and graphite (cathode) were the configurations used to develop the solid state electrochemical cells. Graphite was employed as positive electrode while compounds based on lithium are used as negative electrode. These three elements were combined into a pellet and subjected to multimeter analysis. Table-2 summarizes the evaluation and values for the open circuit voltage (OCV), short circuit current (SCC) and other cell parameters for these cells. The observed discharge capacity around 458 μA at current density 341 μA/cm^2 suggests the SiO_2 doped rGO-WO_3composite electrolyte cells exhibit improved performance and better stability.

TABLE-2
VARIOUS CELL PARAMETERS OF SiO_2 DOPED rGO-WO_3 COMPOSITE ELECTROLYTE

Cell parameters	SiO_2 doped rGO-WO_3 composite electrolyte
Open circuit voltage (OCV)	1.012 V
Short circuit current (SCC)	458 μA
Area of the cell	1.34 cm^2
Weight of the cell	1.28 g
Thickness of the cell	136 μm
T.F. plateau region	78 h
Power density	3.62 W/Kg
Energy density	282.24 Wh/Kg
Current density	341 μA/cm^2

Conclusion

The present work demonstrates eco-friendly, cost-effective approach to prepare SiO_2 doped rGO-WO_3 composite with solid

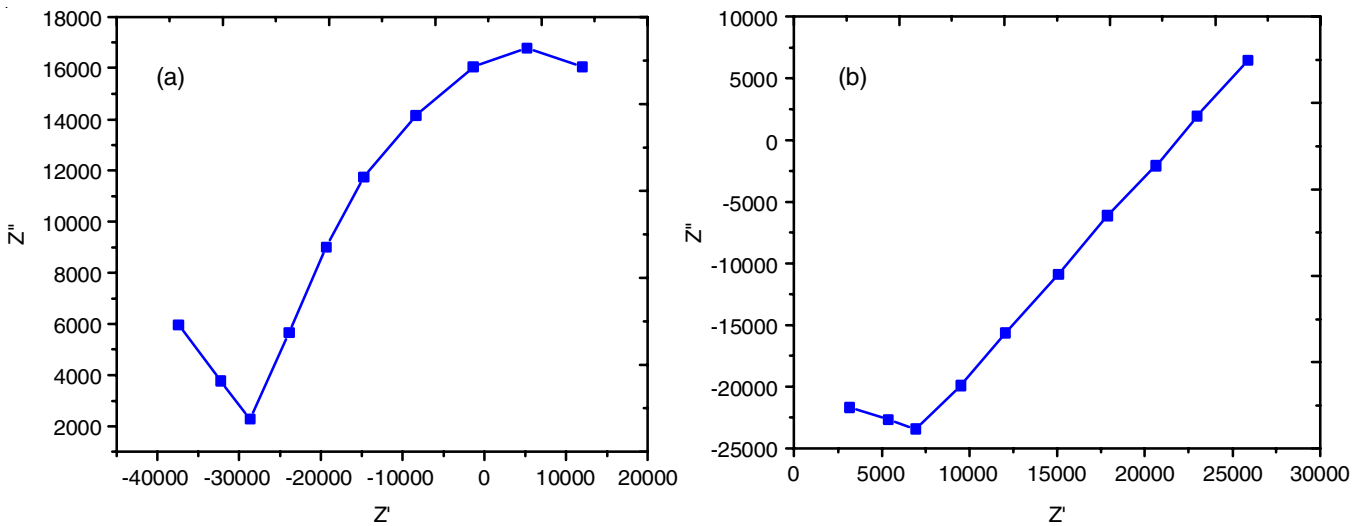

Fig. 5. Nyquist plot of (a) pure WO_3 electrolyte and (b) SiO_2 doped rGO-WO_3 composite

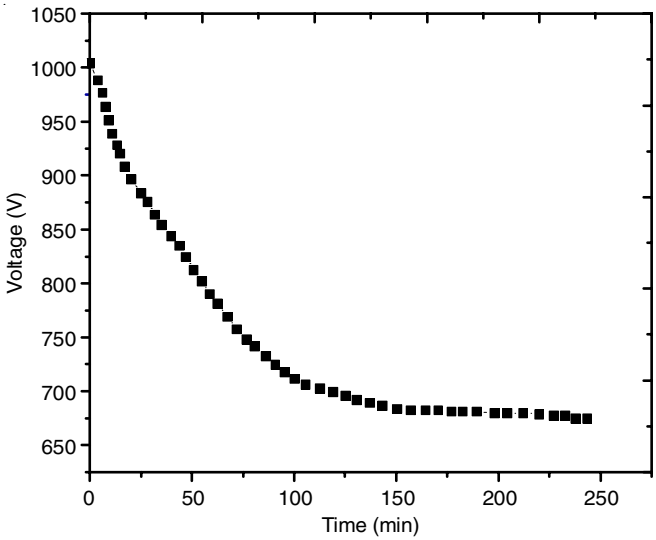

Fig 6. Discharge characteristics of SiO_2 doped rGO-WO_3 composite electrochemical cell electrolyte

state electrode developed by a single-step hydrothermal method. Synthesized SiO_2 doped rGO-WO_3 composite were analyzed using different analytical techniques (XRD, FE-SEM, FT-IR, UV-visible). The synthesis method and annealing temperature were found to have a crystallinity structure with 24 nm average size, porous morphology and efficiency solid state electrode. The XRD spectra exhibited the crystalline peaks of WO_3 nanoparticles, whereas the FE-SEM observations revealed that the synthesized composite have spherical in nature and WO_3 nanoparticles firmly attached on the rGO surface. The UV-visible spectra confirmed the formation of SiO_2 doped rGO-WO_3 composite by the SRP peaks around at 485 nm. At room temperature, the battery exhibits an initial discharge capacity of 458 μA with a current density of 341 μA/cm^2. The SiO_2-doped rGO-WO_3 composite solid state electrode demonstrated an increase in ionic conductivity of 2.74×10^{-5} S cm^{-1} confirmed the efficacy of the novel approach to improve the high-energy materials.

CONFLICT OF INTEREST

The authors declare that there is no conflict of interests regarding the publication of this article.

REFERENCES

1. M. Amir, R.G. Deshmukh, H.M. Khalid, Z. Said, A. Raza, S.M. Muyeen, A.-S. Nizami, R.M. Elavarasan, R. Saidur and K. Sopian, *J. Energy Storage*, **72(E)**, 108694 (2023); https://doi.org/10.1016/j.est.2023.108694
2. V.R. Dharmaraj, Ren-Jei Chung, M.V. Arularasu, T.V. Rajendran and K. Kaviyarasu, *J. Aust. Ceram. Soc*., **59**, 837 (2023); https://doi.org/10.1007/s41779-023-00877-9
3. P. Elayarani, G. Sivakumar, S. Pragadeswaran, S. Sathiyamurthy, T. Sumathi, J. Seshadhri, S. Suthakaran, M. Ayyar and M.V. Arularasu, *Z. Phys. Chem.*, **238**, 1019 (2024); https://doi.org/10.1515/zpch-2023-0531
4. J. Duan, X. Tang, H. Dai, Y. Yang, W. Wu, X. Wei and Y. Huang, *Energ. Rev.*, **3**, 1 (2020); https://doi.org/10.1007/s41918-019-00060-4
5. Y. Liang, C.-Z. Zhao, H. Yuan, Y. Chen, W. Zhang, J.-Q. Huang, D. Yu, Y. Liu, M.-M. Titirici, Y.-L. Chueh, H. Yu and Q. Zhang, *InfoMat*, **1**, 6 (2019); https://doi.org/10.1002/inf2.12000
6. C. Xu, Q. Dai, L. Gaines, M. Hu, A. Tukker and B. Steubing, *Commun. Mater.*, **1**, 99 (2020); https://doi.org/10.1038/s43246-020-00095-x
7. A. Masias, J. Marcicki and W.A. Paxton, *ACS Energy Lett.*, **6**, 621 (2021); https://doi.org/10.1021/acsenergylett.0c02584
8. H. Zhai, T. Gong, B. Xu, Q. Cheng, D. Paley, B. Qie, T. Jin, Z. Fu, L. Tan, Y.H. Lin, C.W. Nan and Y. Yang, *ACS Appl. Mater. Interfaces*, **11**, 28774 (2019); https://doi.org/10.1021/acsami.9b04932
9. L. Mu, Q. Yuan, C. Tian, C. Wei, K. Zhang, J. Liu, P. Pianetta, M.M. Doeff, Y. Liu and F. Lin, *Nat. Commun.*, **9**, 2810 (2018); https://doi.org/10.1038/s41467-018-05172-x
10. Q. Wang, Z. Cui, Q. Zhou, X. Shangguan, X. Du, S. Dong, L. Qiao, S. Huang, X. Liu, K. Tang, X. Zhou and G. Cui, *Energy Storage Mater.*, **25**, 756 (2020); https://doi.org/10.1016/j.ensm.2019.09.010
11. B. Li, Y. Liu, X. Zhang, P. He and H. Zhou, *Green Energy Environ.*, **4**, 3 (2019); https://doi.org/10.1016/j.gee.2018.08.002
12. S.S. Chi, Y.C. Liu, N. Zhao, X. Guo, C.-W. Nan and L.Z. Fan, *Energy Storage Mater.*, **17**, 309 (2019); https://doi.org/10.1016/j.ensm.2018.07.004
13. Y. Zhang, W. Lu, L. Cong, J. Liu, L. Sun, A. Mauger, C.M. Julien, H. Xie and J. Liu, *J. Power Sources*, **420**, 63 (2019); https://doi.org/10.1016/j.jpowsour.2019.02.090
14. R.S. Vemuri, M.H. Engelhard and C.V. Ramana, *ACS Appl. Mater. Interfaces*, **4**, 1371 (2012); https://doi.org/10.1021/am2016409
15. S. Vijayakumar and S. Vadivel, *Opt. Laser Technol.*, **118**, 44 (2019); https://doi.org/10.1016/j.optlastec.2019.04.040
16. X. Zhang, X. Lu, Y. Shen, J. Han, L. Yuan, L. Gong, Z. Xu, X. Bai, M. Wei, Y. Tong, Y. Gao, J. Chen, J. Zhou and Z.L. Wang, *Chem. Commun.*, **47**, 5804 (2011); https://doi.org/10.1039/c1cc10389j
17. W.P. Jakubik, *Thin Solid Films*, **517**, 6188 (2009); https://doi.org/10.1016/j.tsf.2009.04.008
18. M.V. Arularasu, M. Sendhil, T.V. Rajendran, G. Mani, A.M. Aljuwayid and M.A. Habila, *Inorg. Chem. Commun.*, **139**, 109332 (2022); https://doi.org/10.1016/j.inoche.2022.109332
19. M.V. Arularau, *BioNanoSci.*, **14**, 2170 (2024); https://doi.org/10.1007/s12668-024-01541-7
20. X. Chen, Y. Xie, Y. Ling, J. Zhao, Y. Xu, Y. Tong, S. Li and Y. Wang, *Mater. Des.*, **192**, 108760 (2020); https://doi.org/10.1016/j.matdes.2020.108760
21. W. Li, Y. Pang, J. Liu, G. Liu, Y. Wang and Y. Xia, *RSC Adv.*, **7**, 23494 (2017); https://doi.org/10.1039/C7RA02603J
22. M.V. Arularasu, *SN Appl. Sci.*, **1**, 393 (2019); https://doi.org/10.1007/s42452-019-0424-5
23. S. Kalaiarasi and M. Jose, *J. Nanostruct.*, **7**, 47 (2017); https://doi.org/10.1007/s40097-016-0213-2